arXiv:1406.4192v1 [cond-mat.soft] 16 Jun 2014

Microscopic Picture of Cooperative Processes in Restructuring Gel Networks

Jader Colombo,[1] Asaph Widmer-Cooper,[2] and Emanuela Del Gado[1]

[1] *Department of Civil, Environmental and Geomatic Engineering, ETH Zürich, CH-8093 Zürich, Switzerland*
[2] *School of Chemistry, University of Sydney, NSW 2006, Australia*

Colloidal gel networks are disordered elastic solids that can form even in extremely dilute particle suspensions. With interaction strengths comparable to the thermal energy, their stress-bearing network can locally *restructure* via breaking and reforming interparticle bonds. This allows for yielding, self-healing and adaptive mechanics under deformation. Designing such features requires controlling stress-transmission through the complex structure of the gel and this is challenging because the link between local restructuring and overall response of the network is still missing. Here, we use a space resolved analysis of dynamical processes and numerical simulations of a model gel to gain insight into this link. We show that consequences of local bond-breaking propagate along the gel network over distances larger than the average mesh size. This provides the missing microscopic explanation for why non-local constitutive relations are necessary to rationalize the non-trivial mechanical response of colloidal gels.

Colloidal suspensions can solidify even if very diluted, because short-range interactions make particles aggregate into thin stress-bearing structures [1, 2]. As for other network-forming soft materials, including many with important biological functions or technological potential [3, 4], there is still very limited understanding of how local restructuring processes ultimately affect the transmission of stress through the complex microstructure of the network, where weakly connected or soft regions may coexist with stiffer domains. Experiments suggest that cooperative dynamical processes are responsible for the complex mechanics of gels, which combines both liquid-like and solid-like features and can only be rationalized by non-local constitutive relations [5–7], however a microscopic explanation for this behavior is fundamentally lacking. Here we provide such microscopic insight by showing that the breaking of single bonds in the gel network has consequences over large distances, in terms of cooperative particle rearrangements. We do this by studying model restructuring gel networks, via numerical simulations, together with a new space-resolved analysis of dynamical processes.

Experiments revealed that the particle coordination in colloidal gels can be very low (2 to 3) [8] and that the bonds between particles can support significant torques [9], thus imparting local rigidity. Hence we consider a minimal colloidal model with anisotropic interactions that stabilize open particle networks at low volume fraction [10–12]. For a microscopic particle configuration $\{\mathbf{r}_i\}$ the interaction energy is:

$$U(\{\mathbf{r}_i\}) = \epsilon \left[\sum_{i>j} U_2(\mathbf{r}_{ij}/\sigma) + \sum_i \sum_{j>k}^{j,k\neq i} U_3(\mathbf{r}_{ij}/\sigma, \mathbf{r}_{ik}/\sigma) \right] ,$$

where $\mathbf{r}_{ij}$ is the vector connecting particles i and j. U_2 includes a repulsive core and a narrow attractive well, whereas U_3 imposes an angular rigidity [13]. The parameters σ and ϵ define respectively the units of length (equal to the particle diameter) and energy: typical values for a colloidal system are $\sigma = 10 - 100\,\mathrm{nm}$ and $\epsilon = 1 - 100\,k_\mathrm{B}T$, k_B being Boltzmann constant and T room temperature [1, 14, 15]. The unit of time is $\sqrt{m\sigma^2/\epsilon}$, m being the particle mass. We perform molecular dynamics simulations [16] of systems with $N = 4000$ to 16384 particles at number density $\rho = 0.15$, i.e., an approximate volume fraction $\phi \simeq 0.075$, with an interaction strength $\epsilon = 20\,k_\mathrm{B}T$ such that the particles self-assemble into a persistent spanning network. Although very dilute, this model gel responds as a solid under mechanical loading, with a finite elastic modulus [17]. The static structure factor $S(q) = \frac{1}{N}\sum_{j,k} \exp[-i\mathbf{q}\cdot(\mathbf{r}_j - \mathbf{r}_k)]$ in Fig. 1 quantifies spatial correlations between particle positions over distances $\simeq 2\pi/q$ (where q is in units of σ^{-1}), regardless of whether they are connected or not through the network. This simple model gel is made of chains linked by three-coordinated junctions or *nodes*, with a typical mesh size $l^* \simeq$ 3-4σ. $S(q)$ indicates the bonded

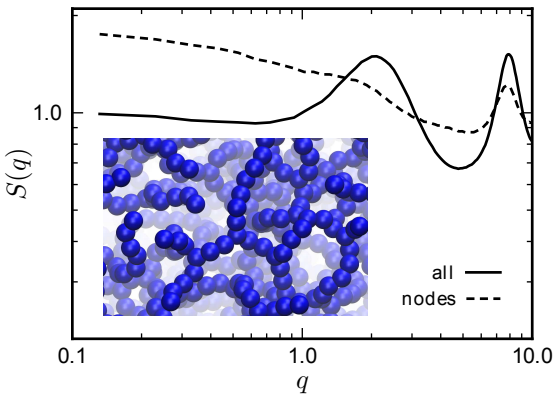

Figure 1. Microstructure of the gel for $\rho = 0.15$ and $\epsilon = 20\,k_\mathrm{B}T$. The static structure factor of the whole system (full line), and of the nodes only (dashed line) are depicted. Inset: real-space image of a section.

particles ($q_b \simeq 8$ corresponds to distances of the order of the typical bond length) and the particles separated by distances $\simeq l^*$ ($q^* \simeq 2$). The contribution to $S(q)$ of the network nodes alone (Fig. 1) indicates long range correlations throughout the network structure (low q) and the presence of clusters of nearby nodes (peak at q_b), suggesting that these are unevenly distributed in space. We measure the density of nodes $c_i^{l_0}$ in the local environment around particle i by counting their number within a distance l_0 corresponding to 5 bonds along the network. Its spatial distribution is indeed highly inhomogeneous, ranging from 0 in loosely connected regions to ≈ 20 in strongly connected ones.

The network *restructures* because thermal fluctuations favor breaking of existing bonds and formation of new ones. The fractions of two- and three- coordinated particles fluctuate about a value that is constant over our simulation time window, and that we use to define the topology of the network. To identify the contribution of the restructuring processes to the dynamical properties of the gel, we compare the restructuring networks to non-restructuring ones, by turning on a barrier in the interaction potential that prevents bonds from breaking [18].

We analyse how the structure changes via the mean degree of self-correlation in particle positions over distances $\simeq 2\pi/q$ and over time t, as measured by the incoherent scattering function $F_s(q,t) = \langle \Phi_s(q,t) \rangle$, where $\langle ... \rangle$ indicates a time average and $\Phi_s(q,t) = \frac{1}{N} \sum_j \exp\left[-i\mathbf{q} \cdot (\mathbf{r}_j(t) - \mathbf{r}_j(0))\right]$. Our data show a strong dependence on the length scale sampled by q and a complex time decay of correlations for wave vectors $q \leq q^* \simeq 2$. Fig. 2A shows $F_s(q,t)$ at $q = 1.0$ (left axis): the two-step decay with a plateau suggests that particles undergo a transient localization process similar to caging in dense glassy suspensions [19]. The decays in the restructuring network (symbols) and the constrained one (dashed line) overlap up to $t_{\rm loc} \simeq 100$. This indicates that the initial decay of correlations is mainly due to motion that is present also in the constrained network and that the plateau value (related to the particle localization) is determined by fixing the network topology (i.e., the mean fractions of 2- and 3- coordinated particles present). The final decay of correlations after the plateau is instead due to the network restructuring. The decay from the plateau is well fitted by a stretched-exponential, $F_s(q,t) \sim \exp[-(t/\tau_q)^\beta]$, with $\beta(q) < 1$ and decreasing to ~ 0.7 with increasing q (Fig. 2B). This qualitative change in the long-time decay, upon varying q, suggests that qualitatively different relaxation processes must come into play over different length-scales. The shape of the decay for $q \leq 2.0$ is typically associated with cooperative dynamics in glassy systems [20]. We characterize this in the gel in a spatially and temporally averaged way using the variance $\chi_4(q,t) = N[\langle |\Phi_s(q,t)|^2 \rangle - \langle \Phi_s(q,t) \rangle^2]$, that quantifies dynamical heterogeneity due to cooperativity. This dynamic susceptibility detects fluctuations from the

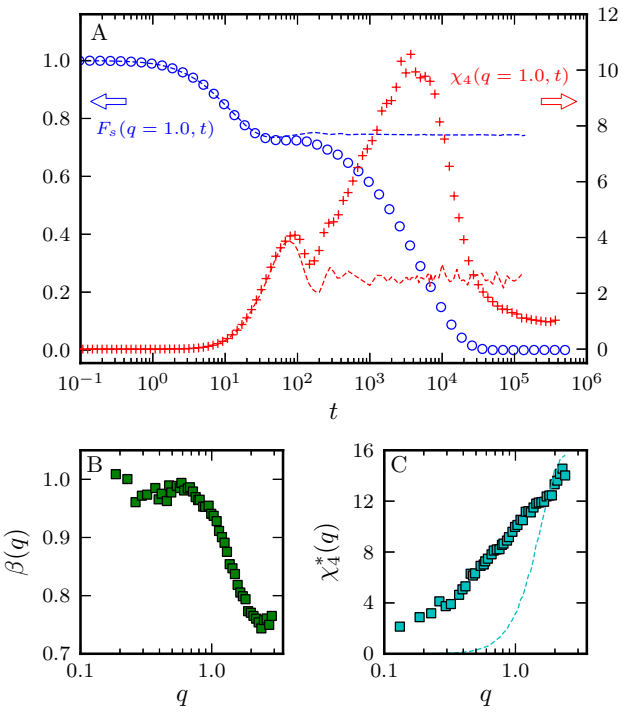

Figure 2. (A): Incoherent scattering function $F_s(q,t)$ (left axis) and variance $\chi_4(q,t)$ (right axis) for $\rho = 0.15$, $\epsilon = 20\,k_{\rm B}T$ and $q = 1.0$, plotted as a function of time, for the restructuring (symbols) and constrained (dashed line) networks; (B): q-dependence of the stretching exponent β; (C): Maximum value $\chi_4^*(q)$ of $\chi_4(q,t)$ over time plotted as a function of q for the restructuring (symbols) and constrained (dashed line) networks.

mean degree of correlation in single particle displacements due to spatial correlations of the dynamics, i.e., to particles undergoing cooperative motion over time t and distance $\simeq 2\pi/q$ [20–22]. Fig. 2A shows $\chi_4(q,t)$ (right axis) for the restructuring (symbols) and constrained networks (dashed line) at $q = 1.0$. The curves coincide up to $t \simeq t_{\rm loc}$ and therefore we can ascribe the initial increase of $\chi_4(q,t)$ to vibrational motion present in both networks. At longer times, in the constrained network $\chi_4(q,t)$ remains constant around its asymptotic value [23, 24]. In contrast, in the restructuring network $\chi_4(q,t)$ develops a significant peak at $t > t_{\rm loc}$ and decays to the asymptotic value of 1 on the same timescale as $F_s(q,t)$ decays to 0, again very similar to what found in dense glassy suspensions [20]. The maximum value of $\chi_4(q,t)$ over time, $\chi_4^*(q)$, increases with the number of particles undergoing cooperative dynamics over length-scales $\simeq 2\pi/q$ [25]. Fig. 2C shows that, for all $q \leq q^* \simeq 2$, it is significantly higher in the restructuring network. Hence the long-time restructuring is cooperative over this range of length-scales.

In order to elucidate how such cooperative processes

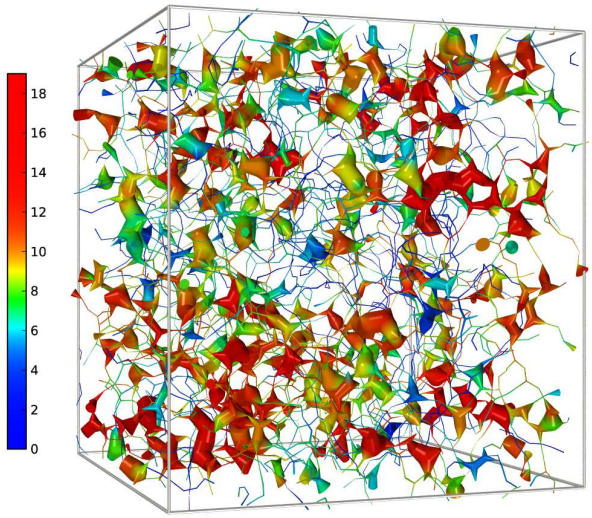

Figure 3. Spatial map of propensity for bond-breaking b_i relative to a time lag $\tau = 10^3$ and a given configuration $\mathscr{C}_0$. The thickness of the segments representing inter-particle bonds is proportional to the propensity for bond-breaking of the bonded particles. The color code represents the local density of nodes $c_i^{l_0}$.

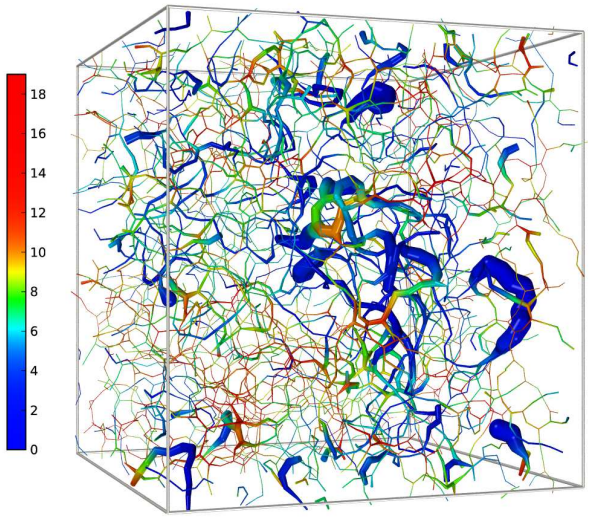

Figure 4. Spatial map of propensity for displacement p_i relative to to the same configuration and time lag as Fig. 3. Segments represent interparticle bonds and their thickness is proportional to the propensity for displacement of the bonded particles. The color code represents the local density of nodes $c_i^{l_0}$.

take place in the gel, we perform a spatially-resolved analysis of the dynamics discussed so far. Let $\mathscr{C}_0 = \{\mathbf{r}_i^0\}$ denote the configuration of the gel, i.e. the set of all particle positions, at time $t = 0$, and let $\mathscr{C}_\tau = \{\mathbf{r}_i^\tau\}$ be the corresponding configuration after an elapsed time interval τ during which the network was able to restructure. The set of particle displacements $\{\mathbf{r}_i^\tau - \mathbf{r}_i^0\}$ is determined not only by the restructuring process, but also by the fast vibrational dynamics. With this in mind we define the sets of *intrinsic* particle positions $\{\hat{\mathbf{r}}_i^0\}$ and $\{\hat{\mathbf{r}}_i^\tau\}$ by constraining the bonds of the corresponding network configuration ($\mathscr{C}_0$ and $\mathscr{C}_\tau$, respectively) and computing the temporally averaged position of each particle over a sufficiently long time window. The intrinsic displacements $\{\hat{\mathbf{r}}_i^\tau - \hat{\mathbf{r}}_i^0\}$ quantify the net effect of restructuring, free from any significant contributions of the network vibrations [17].

We iterate the mapping $\mathscr{C}_0 \to \mathscr{C}_\tau$ starting from the same network configuration $\mathscr{C}_0$ and using different sets of initial particle velocities drawn from a Maxwell-Boltzmann distribution at the same prescribed temperature T. This iso-configurational (IC) ensemble of trajectories allows us to identify, for each particle, its tendency to contribute to specific dynamical processes over a time τ in a way that can be directly related to the microstructure [26–29]. Since we are interested in processes that are relevant to the network restructuring we use $\tau \simeq 10^3$, which corresponds to the time t where $F_s(q^*, t)$ has decayed to $\sim 1/2$ of its value at the plateau (and where $\chi_4(q^*, \tau) \simeq \chi_4^*(q^*)$).

First we use this approach to identify the parts of the structure where bond-breaking, which is responsible for network restructuring, is more likely to occur. This is achieved by defining for each particle i a propensity for bond-breaking $b_i = \langle n_i \rangle_{\mathrm{IC}}$, where $n_i = 1$ if the particle looses, along one of the trajectories, any of the particles bound to it, and 0 otherwise; the angular brackets denote an average over the IC ensemble of trajectories. Fig. 3 shows the spatial distribution of the propensity for bond-breaking for a typical initial configuration: bonded particles are represented by segments of thickness proportional to b_i and colored according to the local density of nodes $c_i^{l_0}$, from dark blue (low $c_i^{l_0}$) to red (high $c_i^{l_0}$). The figure shows that quite unexpectedly bond-breaking events responsible for network restructuring tend to take place in regions with high local density of nodes. We have computed the spatial distribution of local stresses and find that bonds in regions with a higher local density of nodes are indeed subjected to higher-than-average tensile stress [17].

The distribution of intrinsic displacements over our IC ensemble (at the time $\tau = 10^3$) quantifies for each particle its tendency to undergo a significant displacement as a consequence of bond-breaking, thus contributing to the cooperative network restructuring. The second moment $p_i = \left\langle (\hat{\mathbf{r}}_i^\tau - \hat{\mathbf{r}}_i^0)^2 \right\rangle_{\mathrm{IC}}$, which we will call the propensity for displacement of particle i in $\mathscr{C}_0$, provides a spatial map of the effects of bond-breaking events in terms of

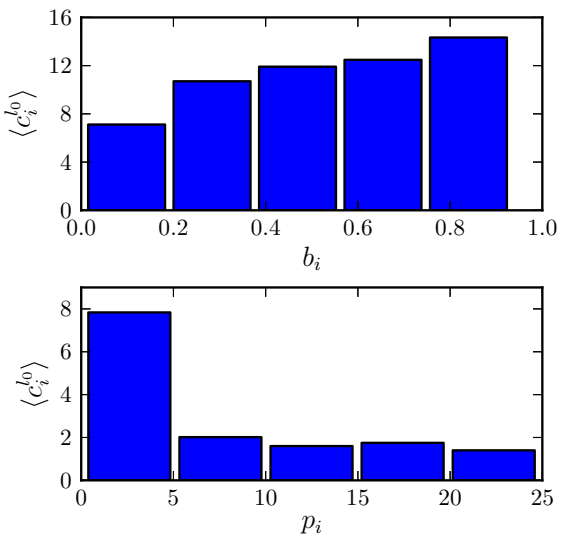

Figure 5. Average local density of nodes $\langle c_i^{l_0} \rangle$ as a function of propensity for bond-breaking b_i (top) and as a function of propensity for displacement p_i (bottom).

intrinsic particle displacements. Fig. 4 shows the spatial distribution of the propensity for displacement for the same initial configuration as in Fig. 3. The thickness of the segments now indicates in which parts of the network the significant displacements responsible for the cooperative restructuring dynamics (Fig. 2) tend to take place. These large intrinsic displacements occur in regions with low local density of nodes, i.e., far away from the bond-breaking events that caused them. We find that these are also the parts of the network more prone to undergo non-affine displacements due to the build-up of internal stresses when the gel is deformed [17]. The cooperative processes we have uncovered are therefore also important for the mechanical response of the gel.

We have quantified these observations by analyzing data obtained from 6 independent initial configurations of a network with 4000 particles, resulting in a set of 24000 triplets $\{c_i^{l_0}, b_i, p_i\}$ [17]. In Fig. 5 we have sorted the particles into five groups according to the values of b_i (top) and p_i (bottom), and plotted for each group the average local density of nodes $c_i^{l_0}$. Quantifying the degree of linear correlation using Pearson's product-moment correlation coefficient [30], we find indeed a negative correlation between p_i and $c_i^{l_0}$ (Pearson's product-moment correlation coefficient $r \simeq -0.35$) and a positive correlation between b_i and $c_i^{l_0}$ ($r \simeq 0.42$).

The picture that emerges is that bond-breaking tends to take place in regions of the network that are more locally connected and experience higher local stresses. Bond-breaking then induces large rearrangements further away, i.e., over length-scales well beyond the network mesh size. These cooperative particle displacements ultimately lead to the network restructuring, characterized by the complex decay of time correlations in the relaxation dynamics [5, 6, 31]. This feedback between local and collective processes, reminiscent of the coupling between particle localization and overall structural relaxation in the dynamics of dense glassy suspensions [32, 33], explains the similarities between dilute gels and dense glasses in the caging processes, two-step decay of time correlations with stretched exponential behavior, and dynamical heterogeneity.

The microscopic picture we obtain is that the gel contains weaker regions (where local stresses are higher and breaking is more likely to occur), which is consistent with arguments made to rationalize the mechanical response of restructuring gels in experiments [4, 15]. We show, however, that the consequences of bond-breaking are non-local, cooperative displacements involving parts of the structure that are relatively far away, in regions where non-affine displacements are more likely to concentrate under deformation. Hence a significantly more complex scenario emerges for the mechanical response, where the mesoscale organization of the gel network has a significant role. Our results suggest that under deformation higher tensile stresses are likely to build up, and favor bond-breaking, in densely connected regions. Moreover, non-affine displacements under deformation are related to the irreversible rearrangements responsible for local plastic events [7, 34] that hinder relaxation of local stresses upon unloading the material. This microscopic, quantitative information, available from our study, on when and where local irreversible events are more likely to occur, can now be incorporated into non-local constitutive models for the viscoelastic response of colloidal gels and similar materials.

This work was supported by Swiss National Science Foundation (SNSF) (Grants No. PP00P2_126483/1 and No. IZK0Z2_141601). A.W. also thanks the Australian Research Council for support.

SUPPLEMENTARY INFORMATION

S1. Mechanical tests

We have carried out non-equilibrium molecular dynamics simulations of a restructuring gel network with $N = 4000$ particles, density $\rho = 0.15$ and an interaction strength $\epsilon = 20\, k_{\mathrm{B}}T$ (reduced temperature $T = 0.05$). The network was sheared in the xz plane with a constant shear rate $\dot{\gamma}$ up to a final strain $\gamma_{xz} = 30\%$, and the shear stress σ_{xz} was recorded. The tests were performed using SLLOD equations of motion [35] implemented in LAMMPS [16], and the temperature was controlled by means of a chain of Nosé-Hoover thermostats. We show results obtained by averaging over a set of 100 independent initial configurations of the network.

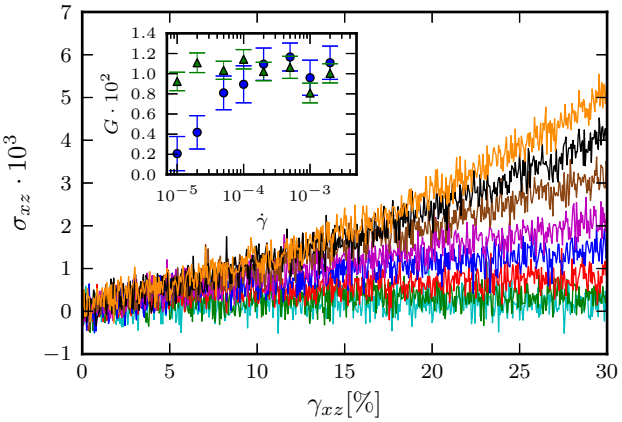

Figure S1. Main plot: shear stress σ_{xz} as a function of shear strain γ_{xz} for different values of the shear rate $\dot{\gamma}$ (from top to bottom: $2 \cdot 10^{-3}$, 10^{-3}, $5 \cdot 10^{-4}$, $2 \cdot 10^{-4}$, 10^{-4}, $5 \cdot 10^{-5}$, $2 \cdot 10^{-5}$, 10^{-5}). Inset: shear modulus as a function of shear rate, obtained by fitting a linear function to the stress-strain curves in the region of small deformation $0 \leq \gamma_{xz} \leq 5\%$ (circles); shear modulus of the non-restructuring network (triangles).

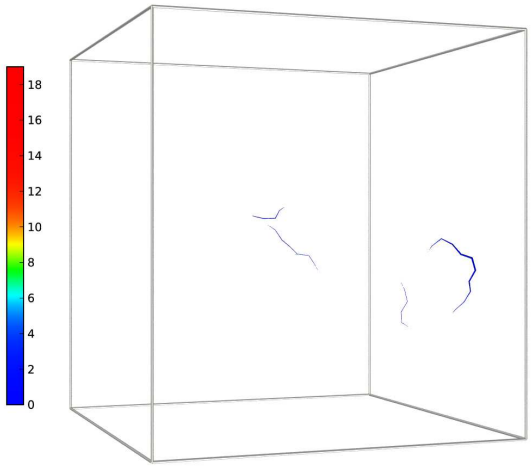

Figure S2. Spatial map of propensity for non-vibrational displacement for the same initial configuration as Figs. 3 and 4 of the main text, but where the bonds have been constrained to not break. Segments represent interparticle bonds and their thickness is proportional to the propensity for displacement of the bonded particles; the scale is the same as in Fig. 4 of the main text. The color code represents the local density of nodes.

The stress-strain curves corresponding to a set of shear rates spanning more than two orders of magnitude – from 10^{-5} to $2 \cdot 10^{-3}$ – are presented in Fig. S1. Although for large deformations the response of the network depends markedly on the shear rate, there exists a linear elastic regime extending approximately up to $\gamma_{xz} \approx 5\%$ from which we can extract a small, but finite shear modulus $G \approx 0.01\,\epsilon/\sigma^3$ for $\dot{\gamma} \geq 5 \cdot 10^{-5}$ (blue circles in the figure inset). Hence our gel network has a solid-like elastic response at relatively low shear rate. In a typical colloidal system characterized by $\epsilon = 50\,k_{\rm B}T$, $\sigma = 100$ nm, this corresponds to a shear modulus $G \approx 2$ Pa, which is consistent with what measured in experiments on dilute colloidal gel networks [1, 14]. For even lower shear rates the modulus drops towards zero, presumably due to thermally activated restructuring of the network. This hypothesis is supported by the comparison with a non-restructuring network, whose shear modulus is approximately constant over the whole range of shear rates investigated (green triangles in the figure inset).

S2. On the propensity for displacement

The iso-configurational analysis was originally introduced for dense glassy alloys [26] and needs to be modified for low-density materials. In our low density gel network the amplitude of particle vibrations at fixed interparticle bonds is far bigger than the amplitude of cage rattling in a typical dense system. In order to study network relaxation one needs a way to filter out these vibrations from the underlying displacements due to restructuring. As described in the main text, we have accomplished this task by associating to any given network configuration an *intrinsic* configuration, that we compute by constraining the inter-particle bonds and evaluating the average position of each particle during a simulation at constant temperature. Since bond-breaking cannot take place, the time evolution samples the vibrational dynamics of the given configuration. We compute the intrinsic positions by averaging over a time window $\Delta t_{\rm av} = 2.5 \cdot 10^4$ in reduced units, which is sufficiently long for most structural correlations to decay to zero in the unconstrained system.

As a demonstration that this approach is able to filter out most of the displacements that are not due to network restructuring, we show in Fig. S2 the result of the iso-configurational analysis performed on a *non-restructuring* network. The network configuration is the same as the one shown in Figs. 3 and 4 of the main text, and the time lag for the isoconfigurational trajectories is likewise $\tau = 10^3$. Ideally, one would expect each particle to display zero propensity for displacement. In practice, a subset of the particles show a small but non-zero propensity: this is due to very slow network rearrangements that do not entail breaking of existing bonds or formation of new bonds, but still affect the average position of some of the particles. For instance, a chain initially confined to a region of space by the surrounding chains can break free of its cage and start to oscillate in a different region: this would affect the average position of the particles in the chain, even though no restructuring – that is no change of

inter-particle bonds – has taken place. The contribution of processes of this latter kind to the propensity, however, are very small compared to the displacements due to restructuring. By comparing the propensity for displacement in the restructuring network, p_i, to the same quantity evaluated in the constrained network, p_i^c, one can define a noise-to-signal ratio as

$$\mathrm{NSR}_p = \frac{1}{N}\sum_{i=1}^{N}\frac{p_i^c}{p_i}\,.$$

For the configuration shown in Fig. S2 the $\mathrm{NSR}_p < 1\%$, i.e. the displacements not directly ascribable to network restructuring contribute on average less than 1% of the total per-particle signal.

S3. Correlation between propensities and local density of nodes

In performing the iso-configurational analysis we have considered six independent configurations of a network with $N = 4000$ particles; for each configuration, an ensemble of 100 trajectories has been generated. This allowed us to associate to each particle i a local density of nodes $c_i^{l_0}$ – a topological attribute of the particle in the initial configuration – as well as the propensities for non-vibrational displacement (p_i) and bond breaking (b_i), which are dynamical properties calculated by averaging over the ensemble of trajectories. In this way we gathered a set of 24000 triplets $\{c_i^{l_0}, p_i, b_i\}$. The raw scatter plots $c_i^{l_0}$ vs. p_i and $c_i^{l_0}$ vs. b_i are shown in Figs. S3 and S4, respectively. It is apparent that particles characterized by a high propensity for displacement tend to be in regions with low density of nodes; in contrast, particles characterized by a high propensity for bond breaking tend to localize in regions with high density of nodes. What is also apparent is that the inverse relationship does not hold, i.e. particles with low (high) $c_i^{l_0}$ often do not have high p_i (b_i). This indicates that the local particle environment is not the only structural property that affects where relaxation takes place.

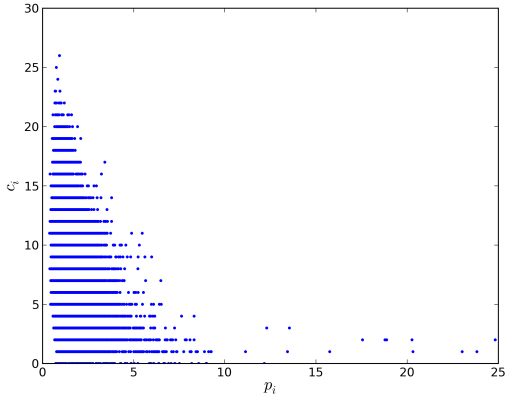

Figure S3. Scatter plot $c_i^{l_0}$ vs. p_i.

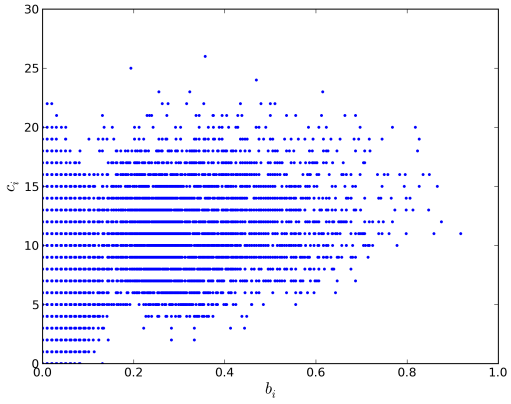

Figure S4. Scatter plot $c_i^{l_0}$ vs. b_i.

S4. Stress distribution

Bond breaking happens preferentially in regions with a high density of nodes (i.e. crosslinks). In order to ascertain whether this is due to a concentration of stresses in those regions, we have calculated the stress distribution in the gel.

Local stresses are obtained by dividing the simulation box into a set of n_c cubic cells, $\{\mathcal{C}_m\}_{m=1\ldots n_c}$, and associating with each cell an average stress tensor $\sigma_{\alpha\beta}^m = \langle s_{\alpha\beta}^m \rangle$, where $s_{\alpha\beta}^m$ is the instantaneous stress tensor corresponding to a specific particle configuration, and the angular brackets denote a time average. The instantaneous stress tensor for each cell is computed according to the standard virial formula [36] in the following way:

$$s_{\alpha\beta}^m = -\frac{1}{V_m}\sum_{i\in\mathcal{C}_m} w_{\alpha\beta}^i\,, \tag{1}$$

where V_m is the cell volume, the sum runs over the particles contained in the cell, and $w_{\alpha\beta}^i$ represents the contribution to the stress tensor of the interactions involving particle i. The latter is defined by splitting the contribution of each interaction evenly among the particles that participate in it:

$$\begin{aligned} w_{\alpha\beta}^i = \frac{1}{2}\sum_{n=1}^{N_2}(r_\alpha^i F_\beta^i + r_\alpha' F_\beta')+ \\ \frac{1}{3}\sum_{n=1}^{N_3}(r_\alpha^i F_\beta^i + r_\alpha' F_\beta' + r_\alpha'' F_\beta'')\,. \end{aligned} \tag{2}$$

In the previous expression the first sum runs over the

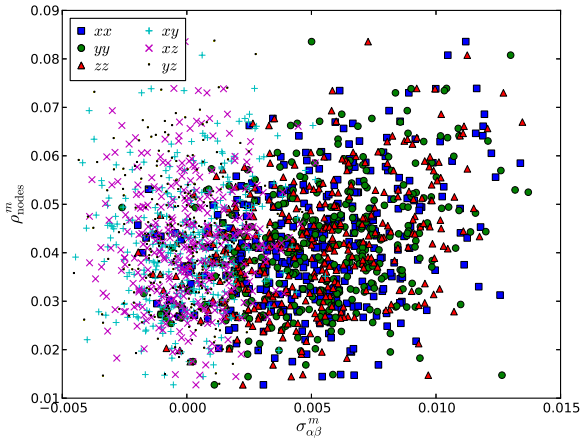

Figure S5. Scatter plot of the components of the local stress tensor $\sigma^m_{\alpha\beta}$ vs. the local density of nodes $\rho^m_{\rm nodes}$.

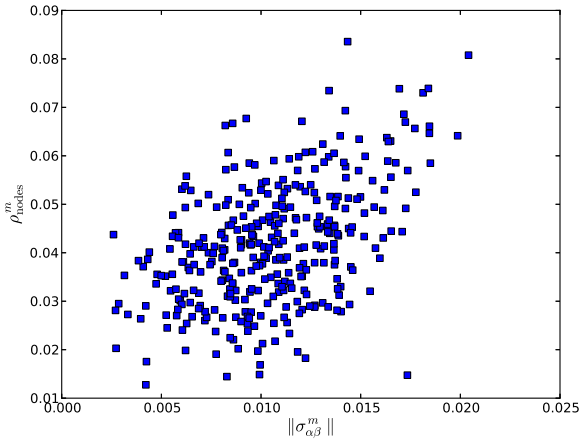

Figure S6. Scatter plot of the norm of the local stress tensor $\|\sigma^m_{\alpha\beta}\|$ vs. the local density of nodes $\rho^m_{\rm nodes}$.

N_2 pair interactions that particle i is part of, $\mathbf{r_i}$ and $\mathbf{r}'$ are the positions of the two interacting particles, and $\mathbf{F_i}$ and $\mathbf{F}'$ are the forces on the two particles resulting from the interaction. Along the same lines the second sum takes into account the N_3 three-body interactions involving particle i. [37]

We have applied the analysis just outlined to a gel network with $N = 16384$ particles, density $\rho = 0.15$ and interaction strength $\epsilon = 20\,k_{\rm B}T$ (reduced temperature $T = 0.05$). The simulation box has been divided in $n_c = 7^3$ cells, so that each cell contains on average around 50 particles. The time window for the temporal averaging has been chosen as $\Delta t = 250$, which is long enough to account for the vibrational dynamics of the network, but yet short enough for the network structure not to be significantly perturbed by the restructuring process (during the prescribed time window less than 5% of the particles change neighbors). For each cell we have also computed the average number density of nodes $\rho^m_{\rm nodes}$, a quantity that measures the local concentration of crosslinks.

In Fig. S5 we show the scatter plot of the components of the local stress tensor vs. the local density of nodes. The shear components xy, xz and yz are on average zero and do not show any particular correlation with the density of nodes. On the contrary, the diagonal components xx, yy and zz are greater than zero and have a positive correlation with the density of nodes. This means that the cells are under isotropic tension, the tension being greater where the density of nodes is higher.

The same trend is evinced from Fig. S6, where the norm of the local stress tensor is plotted vs. the local density of nodes. The positive correlation between the two quantities is assessed by a Pearson's coefficient $r = 0.47$.

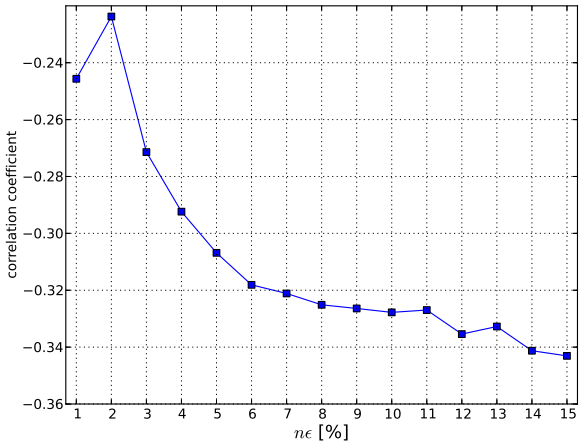

Figure S7. Pearson's coefficient of correlation between the norm of the non-affine displacements and the local density of nodes, $r(\{\|\mathbf{d}_i\|\}_{n\varepsilon}, c_i^{l_0})$, plotted as a function of the strain $n\varepsilon$.

S5. Non-affine displacements

In order to understand which parts of the gel are more prone to displacement as a consequence of internal stresses we have performed a quasi-equilibrium deformation of the network at zero temperature and looked at the non-affine displacement field. The procedure is as follows.

A configuration of the network at finite temperature $\mathscr{C}_0$ is first relaxed to the closest minimum in the potential energy landscape $\tilde{\mathscr{C}}_0$, i.e. the closest "inherent structure", by slowly draining energy from the system by means of a fictitious frictional force proportional to the particles' velocity added on top of the usual interaction. We find this procedure more effective than a direct energy minimization, probably owing to the floppiness of the network

translating into large nearly flat regions in the potential landscape. Denoting with $\mathbb{M}$ the relaxation procedure, we can formally write $\tilde{\mathscr{C}_0} = \mathbb{M}\mathscr{C}_0$.

We then apply a small, instantaneous, homogeneous shear deformation $\mathbb{T}_\varepsilon$ to the simulation box, obtaining the configuration $\mathscr{C}_1 = \mathbb{T}_\varepsilon\tilde{\mathscr{C}_0}$. Finally, we relax the configuration to the nearest inherent structure, obtaining $\tilde{\mathscr{C}_1} = \mathbb{M}\mathscr{C}_1$. The non-affine displacement field induced by the shear strain ε is defined as $\{\mathbf{d}_i\}_\varepsilon = \tilde{\mathscr{C}_1} - \mathscr{C}_1 = \mathbb{M}\mathbb{T}_\varepsilon\tilde{\mathscr{C}_0} - \mathbb{T}_\varepsilon\tilde{\mathscr{C}_0}$, where the difference between configurations is to be understood as the set of differences of the positions of corresponding particles. This basic step can be iterated any number of times to obtain the non-affine displacement field corresponding to a strain $n\varepsilon$: $\{\mathbf{d}_i\}_{n\varepsilon} = (\mathbb{M}\mathbb{T}_\varepsilon)^n\tilde{\mathscr{C}_0} - \mathbb{T}_\varepsilon^n\tilde{\mathscr{C}_0}$.

We have performed the analysis on six independent gel configurations with $N = 4000$ particles, deforming with steps of $\varepsilon = 1\%$ strain, up to a final strain $n\varepsilon = 15\%$. The configurations are the same as the ones used for the iso-configurational analysis. We quantify the correlation between the magnitude of the non-affine displacements and the local density of crosslinks by means of Pearson's coefficient of correlation $r(\{\|\mathbf{d}_i\|\}_{n\varepsilon}; c_i^{l_0})$. The correlation coefficients corresponding to different strains are plotted in Fig. S7. We find a consistent negative correlation, meaning that the larger non-affine displacements happen preferentially in regions with low density of crosslinks.

[1] V. Trappe, V. Prasad, L. Cipelletti, P. Segre, and D. Weitz, Nature **411**, 772 (2001).

[2] P. J. Lu, E. Zaccarelli, F. Ciulla, A. B. Schofield, F. Sciortino, and D. A. Weitz, Nature **453**, 499 (2008).

[3] O. Lieleg, J. Kayser, G. Brambilla, L. Cipelletti, and A. R. Bausch, Nature Materials **10**, 236 (2011).

[4] C. Yan, A. Altunbas, T. Yucel, R. P. Nagarkar, J. P. Schneider, and D. J. Pochan, Soft Matter **6**, 5143 (2010).

[5] A. Duri, D. A. Sessoms, V. Trappe, and L. Cipelletti, Phys. Rev. Lett. **102**, 085702 (2009).

[6] S. Maccarrone, G. Brambilla, O. Pravaz, A. Duri, M. Ciccotti, J. M. Fromental, E. Pashkovski, A. Lips, D. Sessoms, V. Trappe, and L. Cipelletti, Soft Matter **6**, 5514 (2010).

[7] J. Goyon, A. Colin, G. Ovarlez, A. Ajdari, and L. Bocquet, Nature **454**, 84 (2008).

[8] C. J. Dibble, M. Kogan, and M. J. Solomon, Phys. Rev. E **77**, 050401 (2008).

[9] J. Pantina and E. Furst, Phys. Rev. Lett. **94**, 138301 (2005).

[10] E. Del Gado and W. Kob, Phys. Rev. Lett. **98**, 28303 (2007).

[11] S. Saw, N. Ellegaard, W. Kob, and S. Sastry, Phys. Rev. Lett. **103**, 248305 (2009).

[12] M. A. Miller, R. Blaak, C. N. Lumb, and J.-P. Hansen, J. Chem. Phys. **130**, 114507 (2009); B. Capone, I. Coluzza, F. LoVerso, C. N. Likos, and R. Blaak, Phys. Rev. Lett. **109**, 238301 (2012); F. Sciortino and E. Zaccarelli, Curr. Opin. Solid State Mater. Sci. **15**, 246 (2011).

[13] The two- and three-body terms in the interaction potential correspond to $U_2(\mathbf{r}) = A\left(a\,r^{-18} - r^{-16}\right)$ and $U_3(\mathbf{r},\mathbf{r}') = B\,\Lambda(r)\Lambda(r')\,\exp\left[-\left(\frac{\mathbf{r}\cdot\mathbf{r}'}{rr'} - \cos\bar{\theta}\right)^2/w^2\right]$, respectively. The factor $\Lambda(r) = r^{-10}\left[1-(r/2)^{10}\right]^2 H(2-r)$, H being the unit step function, ensures that only triplets of neighbors contribute to the energy. Here we consider $A = 6.27, a = 0.85, B = 67.27, \bar{\theta} = 65^\circ, w = 0.30$.

[14] V. Prasad, V. Trappe, A. D. Dinsmore, P. N. Segre, L. Cipelletti, and D. A. Weitz, Faraday Discuss. **123**, 1 (2003).

[15] M. Laurati, S. Egelhaaf, and G. Petekidis, J. Rheol. **55**, 673 (2011).

[16] S. Plimpton, J. Comp. Phys. **117**, 1 (1995).

[17] See Supplementary Information.

[18] The barrier has the form $U_2^s(\mathbf{r}_{ij}/\sigma) = C\exp\left[-(r_{ij}/\sigma-\gamma)^2/\delta^2\right]$, with $C = 10.0$, $\gamma = 1.2$ and $\delta = 0.01$.

[19] W. Götze, International Series of Monographs on Physics **143** (2009).

[20] L. Berthier, G. Biroli, J.-P. Bouchaud, L. Cipelletti, and W. Van Saarloos, International Series of Monographs on Physics (2011).

[21] C. Donati, S. Franz, S. Glotzer, and G. Parisi, Journal of Non-Crystalline Solids **307**, 215 (2002).

[22] N. Lacevic, F. Starr, T. Schroeder, and S. Glotzer, Journal of Chemical Physics **119**, 7372 (2003).

[23] T. Abete, A. de Candia, E. Del Gado, A. Fierro, and A. Coniglio, Phys. Rev. E **78**, 041404 (2008).

[24] A. Fierro, E. Del Gado, A. de Candia, and A. Coniglio, J. Stat. Mech. , L04002 (2008).

[25] L. Berthier, G. Biroli, J.-P. Bouchaud, W. Kob, K. Miyazaki, and D. Reichmann, J. Chem. Phys. **126**, 184503 (2007).

[26] A. Widmer-Cooper, P. Harrowell, and H. Fynewever, Phys. Rev. Lett. **93**, 135701 (2004).

[27] A. Widmer-Cooper and P. Harrowell, J. Chem. Phys. **126**, 154503 (2007).

[28] A. Widmer-Cooper, H. Perry, P. Harrowell, and D. Reichman, Nature Physics **4**, 711 (2008).

[29] A. Widmer-Cooper, H. Perry, P. Harrowell, and D. R. Reichman, J. Chem. Phys. **131**, 194508 (2009).

[30] J. L. Rodgers and W. A. Nicewander, The American Statistician **42**, 59 (1988).

[31] A. Duri and L. Cipelletti, Europhys. Lett. **76**, 972 (2006).

[32] R. Candelier, A. Widmer-Cooper, J. K. Kummerfeld, O. Dauchot, G. Biroli, P. Harrowell, and D. R. Reichman, Phys. Rev. Lett. **105**, 135702 (2010).

[33] C. De Michele, E. Del Gado, and D. Leporini, Soft Matter **7**, 4025 (2011).

[34] A. Lemaître and C. Caroli, Phys. Rev. E **76**, 036104 (2007).

[35] D. Evans and G. Morriss, *Statistical Mechanics of Nonequilibrium Liquids* (ANU E Press, 2007).

[36] A. P. Thompson, S. J. Plimpton, and W. Mattson, J. Chem. Phys. **131**, 154107 (2009).

[37] The "particle stress" $w^i_{\alpha\beta}$ is readily available in `LAMMPS` thanks to the fix `stress/atom`.